GenX in Water: Interactions and Self-Assembly

Samhitha Kancharla,[1] Aditya Choudhary,[2] Ryan T. Davis,[2] Dengpan Dong,[2] Dmitry Bedrov,[2]* Marina Tsianou,[1]* Paschalis Alexandridis[1]*

1 Department of Chemical and Biological Engineering, University at Buffalo, The State University of New York (SUNY), Buffalo, NY 14260-4200, U.S.A.

2 Department of Materials Science and Engineering, University of Utah, 122 South Central Campus Drive, Room 304, Salt Lake City, UT 84112, U.S.A.

ABSTRACT

2,3,3,3-tetrafluoro-2-(heptafluoropropoxy) propanoate, a.k.a. "GenX", is a surfactant introduced as a safer alternative to replace perfluorooctanoate (PFOA) in the manufacturing of fluorinated polymers, however, GenX is shown to cause adverse health effects similar to, or even worse than, those of the legacy PFOA. With an overarching goal to understand the behavior of GenX molecules in aqueous media, we report here on GenX micelle formation and structure in aqueous solutions, on the basis of results obtained from a combination of experimental techniques such as surface tension, fluorescence, viscosity, and small-angle neutron scattering (SANS), and molecular dynamics (MD) simulations. To our best knowledge, this is the first report on GenX micelles. The critical micelle concentration (CMC) of GenX ammonium salt in water is 175 mM. GenX forms small micelles with association number 6 – 8 and 10 Å radius. GenX molecules prefer to align along the micelle surface, and the ether oxygen of GenX has very little interaction with and exposure to water. Information on the surfactant and interfacial properties of GenX is crucial, since such properties are manifestations of interactions between GenX molecules and between GenX and water molecules and, in turn, the amphiphilic character of GenX dictates its fate and transport in the aqueous environment, its interactions with various biomolecules, and its binding to adsorbent materials.

Keywords: PFAS, fluorocarbon, surfactant, micelle, adsorption, remediation

* Corresponding authors: Paschalis Alexandridis <palexand@buffalo.edu>, Marina Tsianou <mtsianou@buffalo.edu>, Dmitry Bedrov <d.bedrov@utah.edu>

INTRODUCTION

Per- and polyfluoro alkyl substances (PFAS), also called "Forever Chemicals", are a class of synthetic compounds composed of a carbon chain that is fully or partially fluorinated and can be linear or branched. PFAS comprise fluorinated polymers, surfactants, ethers, esters, alcohols and thiols (Buck *et al.*, 2012; Glüge *et al.*, 2020). A major PFAS subgroup are surfactants that consist of a fluorinated hydrophobic tail and a hydrophilic headgroup. The high electronegativity, low polarizability and small size of fluorine give rise to strong C–F bond, weak $–CF_2–$ intermolecular forces, and strong hydrophobic interactions which, in turn, result in PFAS surfactants exhibiting outstanding properties, including incompatibility with both water and hydrocarbons, high wetting ability, and high chemical and thermal stability (Kissa, 2001; Krafft and Riess, 2015). These properties render PFAS surfactants useful in many applications, including nonstick cookware, food packaging paper, stain repellant and waterproof clothing, paints, cosmetics, and firefighting foams (Buck *et al.*, 2012).

Their widespread use in industrial processes and consumer products has resulted in the release of PFAS into the environment (Alves *et al.*, 2020; Brase *et al.*, 2021; Buck *et al.*, 2011; Prevedouros *et al.*, 2006; Xiao, 2017). PFAS are found in waters around the world (Guelfo and Adamson, 2018; Pan *et al.*, 2018). PFAS concentrations several times higher than the lifetime health advisory (70 ng/L for perfluorooctanoate (PFOA) and perfluorooctane sulfonate (PFOS)) recommended by the U.S. Environmental Protection Agency (EPA) (EPA, 2016) have been detected in drinking water in numerous regions, especially near industrial sites that produce or use PFAS, and near many civilian and military airports that use PFAS-containing aqueous film forming foam (AFFF) (Barzen-Hanson *et al.*, 2017; Dauchy *et al.*, 2017; Sun *et al.*, 2016). The main pathways of human exposure to PFAS are the intake of contaminated water and food, and the migration of PFAS from food packaging (pizza boxes, popcorn bags) or cookware (Domingo and Nadal, 2019; Sunderland *et al.*, 2019). PFAS are distributed predominantly to the liver, blood, and kidney, leading to adverse human health effects such as thyroid dysfunction, immune response suppression, kidney disease, altered cholesterol levels or metabolic diseases, reproductive toxicity, neurodevelopmental problems, and various cancers (Brase *et al.*, 2021; Fenton *et al.*, 2021; Sunderland *et al.*, 2019). Consequently, "legacy" PFAS like PFOA, PFOS, and their related compounds have been banned in many countries, including the U.S., and have been included in the International Stockholm

Convention's list of globally restricted Persistent Organic Pollutants (POP) to eliminate their use. In the U.S., EPA is prohibiting companies from manufacturing, processing, or importing products containing certain long-chain PFAS, without prior EPA review and approval (ITRC, 2020).

In response to these restrictions, manufacturers are introducing short chain PFAS and other fluorinated alternatives for commercial applications (Danish-EPA, 2015; Mohamed *et al.*, 2019; Wang *et al.*, 2013). These "emerging" PFAS are categorized into two groups: (i) shorter-chain homologues of long-chain perfluoroalkyl acids and their precursors, e.g., perfluorobutanesulfonic acid, perfluorohexanoic acid, and (ii) functionalized perfluoropolyethers, in particular perfluoroether carboxylic and sulfonic acids (PFECA and PFESA) with acidic functional group attached to a per- or polyfluoroether chain instead of a perfluoroalkyl chain, e.g., GenX from DuPont/Chemours, and ADONA from 3M/Dyneon (Wang *et al.*, 2013).

The tradename "GenX" denotes the PFAS compound ammonium 2,3,3,3-tetrafluoro-2-(heptafluoropropoxy) propanoate) (FRD-902) which is the conjugate base ammonium salt of 2,3,3,3-tetrafluoro-2-(heptafluoropropoxy) propanoic acid (FRD-903), introduced by DuPont in 2009 as a safer replacement of PFOA in the manufacturing of fluoropolymers such as Teflon (Beekman *et al.*, 2016; DuPont, 2010). GenX has received significant attention recently owing to it being detected in the environment (Brandsma *et al.*, 2018; Gebbink *et al.*, 2017; Heydebreck *et al.*, 2015; Hopkins *et al.*, 2018; Sun *et al.*, 2016), and thus raising concern over possible adverse health effects. GenX causes health effects similar to those from legacy PFOA and PFOS (Beekman *et al.*, 2016; Gomis *et al.*, 2018), which include changes in cholesterol levels, reproductive problems, cancer, liver and kidney damage (Beekman *et al.*, 2016; Blake *et al.*, 2020; Brase *et al.*, 2021; Chappell *et al.*, 2020; Conley *et al.*, 2021; Coperchini *et al.*, 2020; Shea, 2018; Sun *et al.*, 2019; Wen *et al.*, 2020). EPA's toxicity assessment for GenX just concluded that there is suggestive evidence of carcinogenic potential of oral exposure to GenX in humans, and GenX is more toxic than the PFOA surfactant it was intended to replace (EPA, 2021). EPA set a safe daily dose of GenX as 3 ng/kg of body weight, and plans to develop drinking water health advisories for GenX in spring 2022 (EPA, 2021).

The studies published so far on GenX address analytical techniques (Mullin *et al.*, 2019; Munoz *et al.*, 2019), distribution in rivers and drinking water near fluoropolymer manufacturing plants (Brandsma *et al.*, 2018; Gebbink *et al.*, 2017; Hopkins *et al.*, 2018; Sun *et al.*, 2016), in global surface waters (Heydebreck *et al.*, 2015; Pan *et al.*, 2018) and in human serum and urine (Kato *et al.*, 2018). Also, toxicology studies (Beekman *et al.*, 2016; Brase *et al.*, 2021; Caverly Rae *et al.*, 2015; Conley *et al.*, 2021; Shea, 2018; Sun *et al.*, 2019), mechanisms of toxicity (Chappell *et al.*, 2020; Wen *et al.*, 2020); development of an oral reference dose (Thompson *et al.*, 2019), binding affinity for proteins (Allendorf *et al.*, 2019; Cheng and Ng, 2018), toxicity and bioconcentration in aquatic organisms (Hoke *et al.*, 2016), toxicity comparison to long-chain PFAS (Blake *et al.*, 2020; Gomis *et al.*, 2018), absorption, distribution, metabolism and elimination profiles in mammals (Gannon *et al.*, 2016), effects on cell-viability, proliferation, DNA-damage (Coperchini *et al.*, 2020). Also, adsorption on activated carbons (AC) (Sun *et al.*, 2016; Wang *et al.*, 2019a), anion-exchange resins (Dixit *et al.*, 2020; Wang *et al.*, 2019a; Wang *et al.*, 2019b), functionalized hydrogels (Ateia *et al.*, 2019; Huang *et al.*, 2018), covalent organic frameworks (Ji *et al.*, 2018), and cyclodextrins (CDs) (Weiss-Errico and O'Shea, 2019), and chemical degradation (Bao *et al.*, 2018; Bentel *et al.*, 2020). The adsorption of GenX is inferred to involve anion exchange, electrostatic and hydrophobic interactions, however, no direct evidence has been reported (Wang *et al.*, 2019a). Competitive adsorption experiments on AC and anion-exchange resins (IRA67 and IRA400) showed that the adsorbed GenX can be replaced by the relatively more hydrophobic PFOA (Wang *et al.*, 2019a; Wang *et al.*, 2019b), which was ascribed to "the ether bond in the GenX molecule may cause the instability of the negatively charged head adsorbed on adsorbent surface, leading to the replacement of the adsorbed GenX by PFOA" (Wang *et al.*, 2019b). The charge density of perfluorinated ether acids (PFEAS) reportedly governs their removal via ion exchange (Dixit *et al.*, 2020). The efficiency of an ion exchange resin (Purolite® A860) to remove from water GenX, perfluoromethoxy butanoic acid (PFMOBA, $CF_3O(CF_2)_3COOH$), and perfluoromethoxy propanoic acid (PFMOPrA, $CF_3OCF(COOH)CF_3$) followed the order of their respective charge densities GenX < PFMOBA < PFMOPrA. Among the investigated short-chain PFAS, GenX has the lowest charge density (13.8 meq/g C) (Dixit *et al.*, 2020).

The physicochemical properties of GenX have attracted rather limited attention. The available literature reports the standard enthalpy of formation, sublimation vapor pressure, and the

adsorption of GenX at the air−water and solid−water interfaces (where the solids tested are natural quartz sand, Eustis soil, Vinton soil, and Qingdao soil; GenX concentration range: $3x10^{-5}$ – 30 mM) (Gomis *et al.*, 2015; Lukyanova and Papina, 2013; Wang and Niven, 2021; Yan *et al.*, 2020; Zhang *et al.*, 2020). GenX is a surfactant, however, its surfactant properties, such as self-assembly into micelles, remain unknown. Information on these is crucial, since such properties are manifestations of molecular interactions between GenX molecules and between GenX and water molecules and, in turn, the amphiphilic character of GenX dictates its fate and transport in the aqueous environment, its interactions with various biomolecules, and its binding to adsorbent materials (Lin *et al.*, 2002).

With an overarching goal to understand the behavior of GenX molecules in aqueous media, we report here the GenX critical micelle concentration (CMC) and micelle structure and interactions in aqueous solutions, on the basis of results obtained from experimental techniques such as surface tension, fluorescence, viscosity, and small-angle neutron scattering (SANS), and from molecular dynamics (MD) simulations. To our best knowledge, this is the first report on GenX micelles.

MATERIALS AND METHODS

Materials

Ammonium 2,3,3,3-tetrafluoro-2-(heptafluoropropoxy) propionate (GenX ammonium salt) ($C_6H_4F_{11}NO_3$, CAS number: 62037-80-3, MW = 347.08 g/mol, 97% purity), also known as ammonium perfluoro(2-methyl-3-oxahexanoate) or ammonium 2-(heptafluoropropoxy) tetrafluoro- propionate, was obtained from SynQuest Laboratories (Alachua, FL, USA) and used as received. Undecafluoro-2-methyl-3-oxahexanoic acid (GenX acid) ($C_6HF_{11}O_3$, CAS number: 13252-13-6, MW = 330.05 g/mol, 97% purity), also known as perfluoro(2-methyl-3-oxahexanoic) acid or 2,3,3,3-tetrafluoro-2-(heptafluoropropoxy)propanoic acid, was obtained from SynQuest Laboratories (Alachua, FL, USA) and used as received. Deuterium oxide (D, 99.9%), (D_2O, MW = 20.03 g/mol, 99.5% purity), also known as deuterated water, was obtained from Cambridge Isotope Laboratories, Inc. (Tewksbury, MA, USA) and used as received. Samples studied by SANS were prepared using D_2O. Samples for surface tension, pyrene fluorescence, and viscosity experiments were prepared using Milli-Q purified water (0.055 μS/cm). All samples were allowed sufficient time to equilibrate following the mixing of ingredients. The GenX ammonium salt concentrations selected for the SANS experiments (500 and 800 mM) are well above the CMC so that GenX micelles are well-defined. These may be high concentrations for GenX present in the environment, but they are relevant to the capture of GenX via adsorption or membranes, where the local concentration can be even higher. Furthermore, the assembly of GenX into micelles is expected (Bodratti *et al.*, 2017) to occur at much lower concentrations in the vicinity of surfaces such as adsorbent materials, mineral particles, or natural organic matter.

Methods

Surface tension: The surface tension of aqueous surfactant solutions was measured at 21 °C by the Wilhelmy plate method using a Kruss model K100 tensiometer. When the surface tension is plotted as a function of surfactant concentration, the surfactant concentration where the surface tension approaches a plateau like region is considered as CMC. The slope of the surface tension vs logarithm of surfactant concentration plot ($d\gamma/d\log C$) determined close to the CMC can be used to estimate surface properties like the maximum surface excess concentration Γ_{max} and the minimum area occupied by a surfactant molecule (A_{min}) at air/liquid interface (Ito *et al.*, 1996; Jin *et al.*, 2005; Prosser and Franses, 2001):

$$\Gamma_{max} = -\frac{1}{2.303nRT}\left(\frac{d\gamma}{dlogC}\right)_{T,P} \quad (1)$$

$$A_{min} = \frac{1}{N\Gamma_{max}} \quad (2)$$

where γ is the surface tension, R is the universal gas constant (8.314 J mol^{-1} K^{-1}), T is absolute temperature, C is surfactant concentration in mM, and N is the Avogadro number (Ito *et al.*, 1996; Jin *et al.*, 2005). The constant n is taken as 2 for surfactants in which the surfactant ion and counterion are monovalent (Jin, *et al.*, 2005).

The tendency of surfactants to self-assemble into structures of specific shape (e.g., sphere, cylinder) can be informed by the critical packing parameter (CPP) which is defined as:

$$CPP = \frac{V_0}{A_{min}l_c} \quad (3)$$

where V_0 is the volume and l_c is the extended length of the surfactant hydrophobic chain (Kronberg *et al.*, 2014; Nagarajan, 2002).

Micropolarity: Pyrene fluorescence was used to study the micropolarity of aqueous surfactant solutions. 2 µL of 1 mM pyrene (Fluka, Buchs, Switzerland) in ethanol was added to 3 g sample solutions. The resulting overall pyrene and ethanol concentrations were about 0.7 µM and 6.7 x 10^{-4} vol %, respectively. Pyrene fluorescence spectra of GenX aqueous solutions were recorded at 22 °C using a Hitachi F-2500 (Stoughton, MA, USA) fluorescence spectrophotometer for 350 – 450 nm emission wavelength. The excitation wavelength of pyrene was λ = 335 nm. The pyrene monomer emission spectrum exhibits a vibronic fine structure, and the ratio of the intensities of first and third vibronic peaks (I_1/I_3) strongly depends on the polarity of its microenvironment (Nivaggioli *et al.*, 1995; Xing *et al.*, 2013; Yang and Alexandridis, 2000). Pyrene is hydrophobic and it tends to move from the aqueous phase to a hydrophobic environment above the CMC, which is reflected in a decrease in I_1/I_3 values. The concentration value obtained from the intersection of straight lines fitted to the first plateau region of the I_1/I_3 vs. surfactant concentration curve and to the linear part of I_1/I_3 decrease region (near the inflection point) provided CMC values that are consistent with those obtained from surface tension (Kancharla *et al.*, 2019).

Viscosity: The viscosity of aqueous surfactant solutions was measured using Cannon-Fenske capillary viscometer of size 50 (Cannon Instrument Co, State College, PA). The kinematic

viscosity (η) is calculated by multiplying the efflux time with the viscometer calibration constant (provided by the manufacturer). The ratio of the kinematic viscosity of the solution (η) and the kinematic viscosity of pure solvent (η_o) gives the relative viscosity ($\eta_r = \eta/\eta_o$) of the solution. η_r can be expressed in terms of the volume fraction of micelles (φ) (Kancharla *et al.*, 2019; Nagarajan, 1982; Zoeller and Blankschtein, 1998):

$$\eta_r = 1 + \nu\phi + k_1(\nu\phi)^2 + O(\phi)^3 \quad (4)$$

where ν is a shape factor representing the micelle shape and k_1 a coefficient corresponding to pair-wise hydrodynamic interactions between micelles (Zoeller and Blankschtein, 1998). The term $k_1(\nu\phi)^2$ accounts for hydrodynamic interactions, and the term $O(\phi)^3$ arises due to direct micelle-to-micelle interactions and can be neglected for dilute solutions (Nagarajan, 1982; Zoeller and Blankschtein, 1998). The volume fraction of micelles which includes the water of hydration associated with micelles is given by $\phi = V_s^{hyd}(c_s - c_1)$, where V_s^{hyd} is the hydrated volume of a surfactant molecule, c_s total surfactant concentration, and c_1 concentration of unassociated surfactant (taken to be the CMC) (Zoeller and Blankschtein, 1998). For spherical micelles, the shape factor ν is considered to be 2.5 (Nagarajan, 1982; Zoeller and Blankschtein, 1998). We used this value since the GenX micelles are approximately spherical.

Small-angle neutron scattering (SANS): SANS has been widely used to determine the size and structure of surfactant micelles (Berr and Jones, 1989; Burkitt *et al.*, 1987; Fajalia and Tsianou, 2014; Iijima *et al.*, 1998; Kancharla *et al.*, 2022). SANS measurements of aqueous GenX ammonium salt solutions were performed on the NG-7 30 m SANS instruments at the Center for Neutron Research (NCNR), National Institute of Standards and Technology (NIST), Gaithersburg, MD. Neutrons with 6 Å wavelength were focused on samples kept in quartz cells of 2 mm thickness. Sample-to-detector distances (SDD) of 2, 6.5 or 10 m were used for each sample in order to cover the wave vector (q) range 0.01 $Å^{-1}$ < q < 0.35 $Å^{-1}$. The measurement time was in the range 180 – 7200 seconds. Procedures for the treatment of raw SANS intensity data are described elsewhere (Dong *et al.*, 2021; Kancharla *et al.*, 2021a).

SANS data from GenX micelles in D_2O have been fitted with the monodisperse core-shell ellipsoid form factor and the Hayter – Penfold structure factor with rescaled mean spherical approximation (RMSA) (Fajalia and Tsianou, 2014). The ellipsoid shape is consistent with the findings from MD

reported in this study, and encountered in typical PFAS surfactants (Dong *et al.*, 2021; Kancharla *et al.*, 2021a; Kancharla *et al.*, 2021b). The overall scattering intensity I(q) is given by:

$$I_{micelle}(q) = A.\phi.P(q).S(q) + B_{inc} \quad (5)$$

P(q) is the form factor representing the shape and structure of a micelle, while S(q) is the structure factor representing the intermicelle interactions in the solution. φ is the volume fraction of the micelles which in turn depends on the overall surfactant concentration. The parameters A and B_{inc} account for additional contributions due to the absolute scaling and incoherent noise, respectively. The form factor and structure factor models employed here are presented in detail in SI. The major fitting parameters to describe scattering from GenX micelles in D_2O are the surfactant association number (N_{agg}), micelle volume fraction (φ), and charge on a micelle (Z).

The micelle core minor radius (b) was taken to be the extended length of $CF_3(CF_2)_2OCF$: $l_{f,c}$ = 8.0 Å (calculated from atom-atom distances in GenX molecule provided by MD). The volume of the micelle core V_{core} (in $Å^3$) was calculated given the surfactant association number N_{agg} using:

$$V_{core} = N_{agg}(V_{t,GenX} + N_{H,O}V_{D_2O}) \quad (6)$$

where $V_{t,GenX}$ = 200.66 $Å^3$ is the volume of a $CF_3(CF_2)_2OCF$ chain, $N_{H,O}$ is the number of water molecules hydrating the $CF_3(CF_2)_2OCF$ chain in the micelle core, and V_{D_2O} is the volume of a D_2O molecule (Kancharla*, et al.*, 2019).

The volume of the micelle shell, considering its contents: hydrophilic headgroups of the surfactant, CF_3 branch, counterions, and associated water molecules, can be written as:

$$V_{shell} = N_{agg}\left(V_{COO^-} + V_{CF_3} + (1-\alpha)V_{NH_4^+} + N_H V_{D_2O}\right) \quad (7)$$

where V_{COO^-} is the volume of the GenX hydrophilic headgroup, V_{CF_3} volume of the CF_3 group, $V_{NH_4^+}$ volume of the counterion NH_4^+, and N_H hydration number, i.e., number of water molecules associated per surfactant molecule. α = Z/ N_{agg} is the fractional charge on a micelle.

The scattering length density of the micelle core is calculated by equation (8)

$$\rho_{core} = \frac{N_{agg}(b_{CF_3(CF_2)_2OCF} + N_{H,O}b_{D_2O})}{V_{core}} \quad (8)$$

where b_i is the coherent scattering length of molecule i. b_i values are reported in Table S1.

The scattering length density of the micelle shell is calculated using equation (9), which includes the individual contributions to the scattering from surfactant headgroups, CF_3 groups, counterions, and associated water molecules:

$$\rho_{shell} = \frac{N_{agg}\left[b_{COO^-} + b_{CF_3} + (1-\alpha)b_{NH_4^+} + N_H b_{D_2O}\right]}{V_{shell}} \quad (9)$$

The scattering length density of the solvent $\rho_{solvent}$ was calculated using the scattering lengths and concentrations of surfactant and heavy water. The concentration of the GenX ammonium salt present in the bulk solution was considered as its CMC (obtained from pyrene fluorescence). The dielectric constant of water was obtained from literature (Malmberg, 1958).

SANS data originating from GenX micelles in D_2O have also been fitted with other form factor models, including the monodisperse sphere form factor, monodisperse or polydisperse core-shell sphere form factor, and the Hayter – Penfold structure factor with RMSA. The expressions describing these form factor models and micelle structure/composition, SANS fits and important parameters are presented in the SI document. Here we discuss results from what we consider to be the better representation of micelles among all those we tested.

Molecular dynamics (MD) simulations: MD simulations were preformed using an in-house simulation package that utilizes a non-polarizable version of the Atomistic Polarizable Potentials for Liquids, Electrolytes and Polymers (APPLE&P) force field (Bedrov *et al.*, 2019; Borodin, 2009). The parameters for the APPLE&P force field were derived based on fitting an extensive database of ab initio calculations of binding and conformational energies for a variety of small molecule clusters and representative oligomers, as well as systematic empirical adjustments to reproduce a variety of experimentally measured thermodynamic, dynamics, and structural characteristics in various systems. A periodic cubic simulation cell contained 32 GenX and ammonium pairs dissolved in 4032 water molecules (Figure 1), which corresponds to a surfactant concentration of about 440 mM (which is well above the experimentally determined CMC of GenX in water). In the initial configuration, all molecules were distributed homogeneously in a large simulation cell of size 800 Å in each direction, which was subsequently shrunk over 30 ps to

achieve a reasonable density. Then the system was equilibrated in the NPT ensemble for 20 ns, followed by production runs of up to 100 ns.

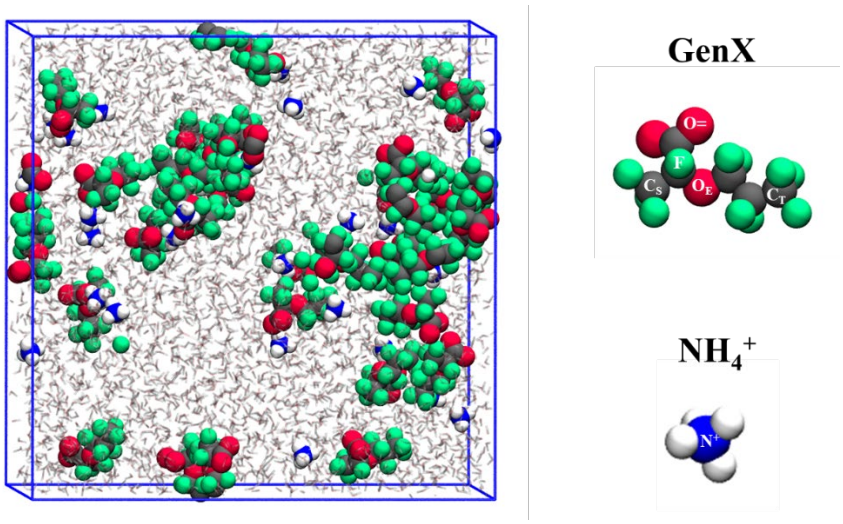

Figure 1. A typical snapshot of the equilibrated system containing GenX and ammonium ions, and water as a solvent. (Carbon-grey; Oxygen-red; Fluorine-green; Nitrogen-blue; Hydrogen-white)

During the simulation, a temperature of 300 K was maintained by employing the Nosé−Hoover thermostat (Hoover, 1985) (coupling frequency 0.01 fs^{-1}) and barostat (coupling frequency 0.0005 fs^{-1}). A cut-off distance of 15.0 Å was set for computing van der Waals interactions and electrostatic interactions in the real space. The Ewald summation method was utilized for the calculation of the reciprocal space contribution to electrostatic interactions. All bonds were constrained using the SHAKE algorithm (Palmer, 1993). A multiple time-step integration scheme (Martyna *et al.*, 1996) was used with the small step (0.5 fs) for calculating bonds and bends, a medium step (1.5 fs) for calculating torsions and short range non-bonded interactions, and a large step (3 fs) for calculating long-range non-bonded interactions and the reciprocal part of Ewald summation. This protocol and force field have been successfully used in our previous simulations of perfluorinated surfactants in aqueous solutions, and have shown good consistency with experimental data characterizing their self-assembly and micellar structure (Dong *et al.*, 2021; Kancharla *et al.*, 2021a).

RESULTS AND DISCUSSION

The association behavior of GenX in aqueous solution is revealed here from combined experimental measurements and atomistic MD simulations. The critical micelle concentration (CMC), surface area per GenX headgroup, and micelle hydration are determined from analysis of surface tension, pyrene fluorescence spectroscopy and viscosity data. Structural information such as the GenX micelle shape, size, and composition is obtained from complementary analysis of MD and SANS data. MD simulations provided additional molecular-level insights into the GenX self-assembly and intermolecular interactions. There is no information available in the literature on GenX surfactant properties, such as self-assembly into micelles or micelle structure.

Premicellar Region and Onset of Micelle Formation

Surface tension data of GenX acid or GenX ammonium salt in aqueous solution are plotted in Figure 2 as a function of surfactant concentration. For GenX acid aqueous solution, the slope ($d\gamma/d\log C$) determined close to the CMC is -30.12 mN/m, Γ_{max} calculated from Equation (1) is 2.67 x 10^{-10} mol cm^{-2}, and A_{min} is 62.1 $Å^2$. For GenX ammonium salt aqueous solution, ($d\gamma/d\log C$) = -23.01 mN/m, Γ_{max} = 2.04 x 10^{-10} mol cm^{-2}, and A_{min} = 81.3 $Å^2$. Interfacial tension parameters are important in the atmospheric transport of PFAS, and in PFAS retention and transport in natural porous media (Brusseau, 2019); also in PFAS treatment and remediation processes (Lee *et al.*, 2017; Meng*, et al.*, 2014).

It is appropriate to compare the properties of GenX to properties of PFAS surfactants that have (i) the same number of carbons with GenX, sodium perfluorohexanoate (NaPFHx, $C_5F_{11}COONa$), and (ii) the same counterion, ammonium perfluorooctanoate (APFO, $C_7F_{15}COONH_4$) (Kancharla *et al.*, 2019). The surface area per headgroup of the GenX acid is close to that of NaPFHx (A_{min} = 63.4 $Å^2$) (Kancharla *et al.*, 2021b) and APFO (64.0 $Å^2$) (Kancharla *et al.*, 2019), whereas the surface area per headgroup of the GenX ammonium salt is 30% greater than that of NaPFHx and APFO.

CPP values are calculated for GenX acid and GenX ammonium salt considering the volume of surfactant hydrophobic chain (V_0) equal to the volume of a $CF_3(CF_2)_2OCF$ chain = 200.7 $Å^3$ (leaving out the CF_3 side-group of GenX molecule, as intimated by MD results presented below),

and the extended length of a $CF_3(CF_2)_2OCF$ chain l_c = 8.0 Å (obtained by MD), are 0.40 and 0.31, respectively. The CPP value 0.31 suggests spherical micelles (CPP<0.33) for GenX ammonium salt. CPP = 0.40 suggests that GenX acid forms cylindrical micelles (0.33<CPP<0.5).

The CMC value obtained from surface tension for GenX acid and GenX ammonium salt in aqueous solution is 150 ± 10 mM and 150 ± 50 mM, respectively. The surface tension of GenX acid remained constant above the CMC, however, for GenX ammonium salt, a dip and subsequent slight increase in the surface tension is observed. The concentration of GenX ammonium salt at the dip where the surface tension is lowest is considered to be the CMC. The origin of the increase in the surface tension above the CMC has not been established here, but it does not affect the analysis of the surface tension data to obtain Γ_{max} and A_{min}.

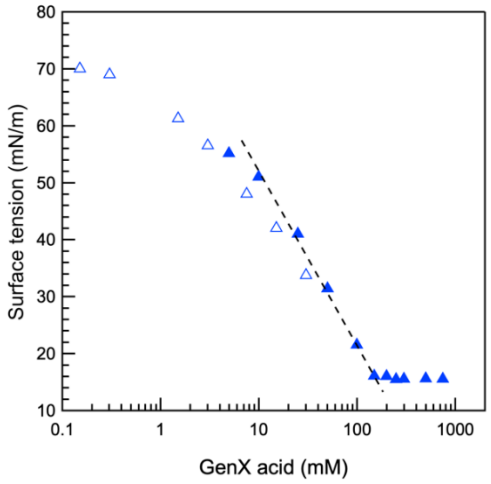

(a)

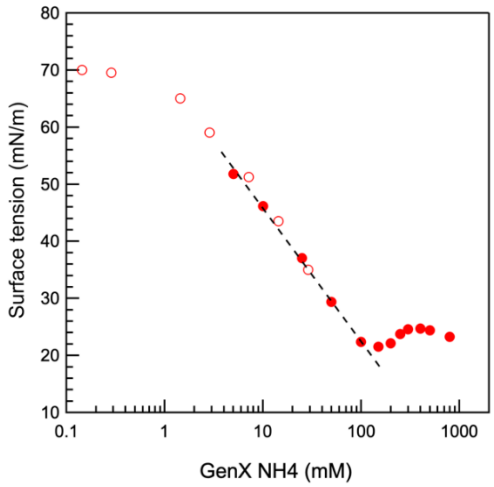

(b)

Figure 2. Surface tension of (a) GenX acid (20.5 °C) and (b) GenX ammonium salt (23.5 °C) aqueous solutions, plotted as a function of surfactant concentration. The surface tension data at low surfactant concentrations (open symbols) were taken from reference (Yan *et al.*, 2020). Linear fits have been applied to the data points where the surface tension decreases prior to reaching the CMC.

Pyrene fluorescence is used to also obtain CMC and, further, assess the polarity of the GenX micelle microenvironment. The I_1/I_3 ratio of GenX acid or GenX ammonium salt aqueous solutions decreased above the CMC due to the partition of pyrene from the polar aqueous solution to the GenX micellar environment (Figure 3). Similar behavior has been previously observed with pyrene for other fluorinated surfactants including PFOA (Dong *et al.*, 2021; Kalyanasundaram, 1988; Muto *et al.*, 1987), which was ascribed to the pyrene molecules residing in the outer palisade layer of the surfactant micelles due to the immiscibility between pyrene and the fluorocarbon core (Xing *et al.*, 2013). The CMC of GenX acid and GenX ammonium salt in aqueous solution obtained from pyrene fluorescence are 140 ± 5 mM and 175 ± 5 mM, respectively. Above CMC, the I_1/I_3 ratio of GenX ammonium salt aqueous solutions at a particular concentration is lower than the I_1/I_3 ratio of NaPFHx solutions (Figure S1). This indicates that GenX micelles offer a more hydrophobic environment for pyrene, presumably allowing more contact between pyrene and fluorocarbon chains. The CMC reported in the literature for the 6-carbon fluorinated surfactants perfluorohexane sulfonic acid (PFHxS, $C_6F_{13}SO_3H$) is 12 mM, perfluorohexanoic acid (PFHxA, $C_5F_{11}COOH$) is 82 mM, and sodium perfluorohexanoate (NaPFHx, $C_5F_{11}COONa$) is 200 mM (Alves *et al.*, 2020; Kancharla *et al.*, 2021b). The CMC of GenX ammonium salt is close to the CMC of NaPFHx. The low CMC of PFHxS compared to PFHxA is due to the presence of 6 carbon atoms in fluorocarbon chain of PFHxS (more hydrophobic), while PFHxA has 5 carbon atoms. The CMC of GenX acid

is greater than the CMC of PFHxA, whereas the CMC of GenX ammonium salt is slightly lower than the NaPFHx CMC. GenX acid and PFHxA have the same headgroup and counterion. Therefore, the difference in the CMC of GenX acid and PFHxA is due to the difference between the perfluoroalkyl chain in PFHxA and the perfluoroether chain in GenX acid. When the counterion is changed, the CMC trend became the opposite. The contribution of micellization of the GenX fluorocarbon chain is assessed next.

The Gibbs free energy of micellization (ΔG_{mic}) is the net free-energy gain for transferring a free surfactant molecule and its counterion from the bulk aqueous solution into a micelle. ΔG_{mic} includes various contributions, the most important of which account for formation of the hydrophobic micelle core, and electrostatic interactions in the micelle shell (Kancharla *et al.*, 2021b). For ionic surfactants, ΔG_{mic} is related to CMC according to $\Delta G_{mic} = (2- \alpha)RTlnX_{CMC}$, where X_{CMC} is the surfactant mole fraction at the CMC, and α the degree of counterion dissociation (Kancharla *et al.*, 2021b). For GenX ammonium salt, ΔG_{mic} = -18.0 kJ/mol considering α = 0.72 (obtained from SANS fits presented later). ΔG_{mic} = -17.9 kJ/mol for NaPFHx, while the free energy contribution due to the formation of the micelle hydrophobic core is -17.5 kJ/mol (Kancharla *et al.*, 2021b). For APFO (CMC = 26.5 mM, α = 0.47) (Kancharla *et al.*, 2019) the electrostatic free energy is -8.1 kJ/mol (Kancharla *et al.*, 2021b). Since GenX ammonium salt and APFO have the same counterion, we assumed the electrostatic free energy of GenX ammonium salt equal to that of APFO, and calculated (following the procedure described in (Kancharla *et al.*, 2021b)) at -4.3 kJ/mol the free energy contributions related to the formation of the GenX ammonium salt micelle hydrated shell and entropy lost by the counterions upon binding onto the micelle charged surface. Subtracting this value from ΔG_{mic} of GenX ammonium salt gives -13.7 kJ/mol for the free energy associated with the formation of the GenX micelle hydrophobic core. Whereas the ΔG_{mic} values of GenX ammonium salt and NaPFHx are almost the same, the free energy associated with the formation of the micelle hydrophobic core is 30% less negative for the ether-containing GenX compared to NaPFHx with linear fluorocarbon chain.

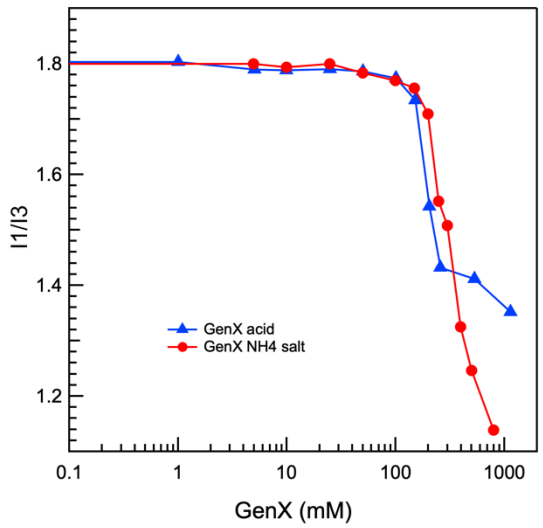

Figure 3. Pyrene fluorescence intensity I_1/I_3 ratio of GenX acid and GenX ammonium salt aqueous solutions (22 °C).

Micelle Structure

In order to understand the structure of GenX miclles in water, we synthesize in this section discussion of results from atomistic MD simulations and SANS analysis. First we discuss the micelle shape and size, and then present information on molecular arrangements inside the micelle.

MD simulations analysis. A broad range of micelle association numbers (i.e., number of surfactant molecules in a micelle) has been observed in MD simulations. A GenX molecule is considered here to be a part of a micelle/cluster only when any of its atoms lie within a cutoff distance of 5.0 Å from any atom of another GenX molecule belonging to the same micelle. We set up two systems with different initial distributions of GenX molecules. In one, the GenX molecules were randomly distributed through the system without forming clusters; in another, they were biased to belong in one large micelle. After 20 ns equilibration, both systems show similar micelle size distributions, with about 30-33% of GenX molecules present as unimers or dimers, and the remaining GenX molecules distributed between micelles of association number N_{agg} = 3 - 25. Unfortunately, the relatively small size of investigated system (i.e., 32 surfactant molecules) and the slow kinetics of micelle formation/breaking (particularly for larger micelles) do not lead to a converged micelle size distribution even from a 100 ns long trajectory. The micellar size distribution and kinetics of micelle formation and dissociation will be addressed in future work. Nevertheless, the population

of unimers shows steady fluctuation around 24% (see Supplemetary Information). Given the 440 mM surfactant concentration in MD simulations, the fraction of unimers observed in MD is in good aggrement with the experimentally determined value of the GenX CMC (150 mM).

While we cannot conclude on equilibrium size distribution of micelles from MD simulation, we have sufficient statistics to analyze the micellar structure and shape for different size micelles observed in our simulations. First, we characterized the shape and dimensions of the formed micelles by calculating the micellar gyration tensor using the following equation:

$$S_{xy}^2 = \frac{1}{M} < \sum_{i=1}^{N} m_i x_i y_i > \quad (10)$$

where N is the number of atoms in a micelle, M total mass of the micelle, x_i, y_i coordinates of atom i relative to the micelle center-of-mass, m_i corresponding mass of atom i, and <> denotes averaging over the entire trajectory. Diagonalization of the gyration tensor matrix yields the principal moments, i.e., S_{xx}, S_{yy}, S_{zz} that can be related to the radius of gyration (R_g) as: $R_g^2 = S^2_{xx} + S^2_{yy} + S^2_{zz}$. The calculated R_g^2 and the corresponding components of the gyration tensor are plotted in Figure 4a as the function of micelle association number. As expected, the R_g^2 and the principal moments monotonically increase with increasing micelle size. Furthermore, Figure 4b clearly shows that the GenX micelles are not spherical, as one of the principal moments of gyration tensor is substantially larger than the other two (S_{zz}/S_{xx}>2.1 and S_{zz}/S_{yy} >1.6), corresponding to a prolate shape of the micelle. The ellipsoidal micellar shape observed in MD allowed us to select the core-shell ellipsoid form factor for fitting SANS data (see discussion below).

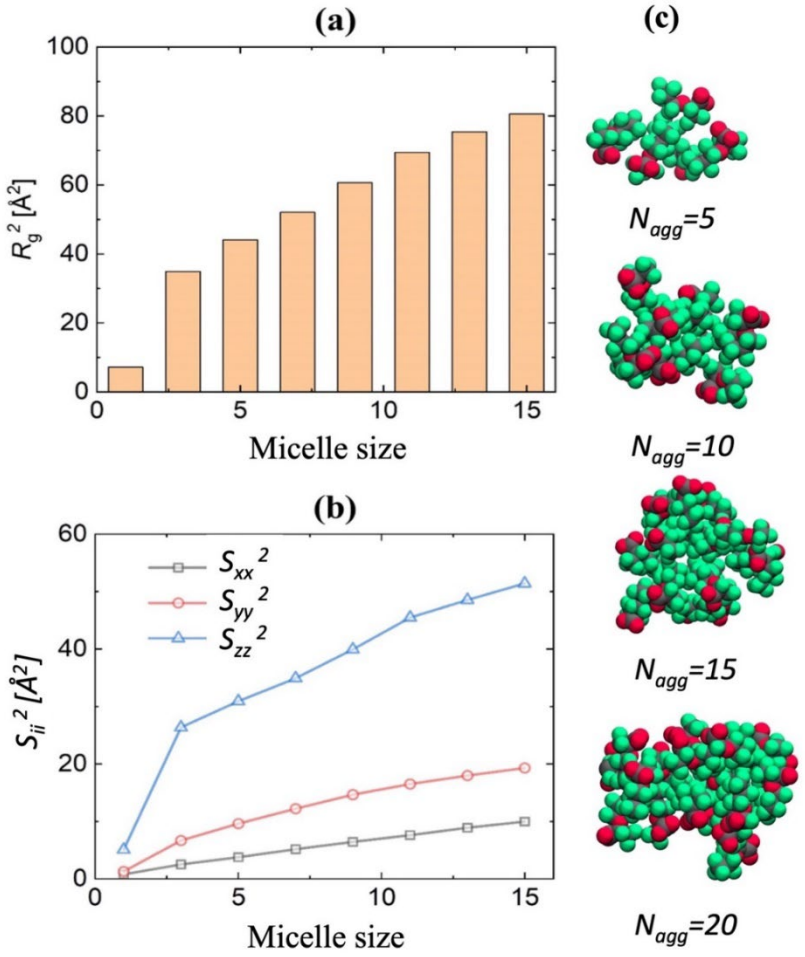

Figure 4. (a) Average R_g^2 of a GenX micelle as a function of micelle association number, (b) principal moments of the gyration tensor as a function of micelle association number, and (c) representative snapshots of several GenX micelles of different association numbers observed in MD simulations.

To understand the structure of individual micelles, we have examined the interaction with water of different parts of the GenX molecule, and their distribution inside the micelle. Figure 5 shows several radial distribution functions ($g(r)$) which reflect the propability of finding a specific atom (e.g., oxygen of water molecule) at a sertain distance r from the selected atom (e.g., oxygen of GenX), and the corresponding coordination numbers (CN) for the selected atom types identified in Figure 5a: O_W is water oxygen atom, O= oxygen atom of GenX headgroup, O_E ether oxygen atom of GenX fluorinated tail, C_T CF_3 carbon at the end of the fluorinated tail, and C_S CF_3 carbon on the side group connected to the GenX headgroup. The first coordination shell is typically defined by the first minimum in $g(r)$ (e.g., r = 3.65 Å for O GenX – O water correlation shown in

Figure 5b), and the number of different atoms in that shell (i.e., CN) provides a good description of the local environment. As expected, a sharp peak for O= - O_W pair and CN=3.2 for the first coordination shell (defined as a sphere with r =3.65 Å) in Figure 5b confirms a strong interaction of water moleules with the GenX anionic headgroup. On the other hand, the ether oxygen has very little interaction with water (note the absense of a strong peak at short distances and CN=0.1 within the first coordination shell r=3.65 Å), indicating that it is sterically hindered from water by fluorinated groups and the headgroup. Figure 5c shows that the g(r) and CN of O_W around the CF_3 carbon atoms of fluoroalkyl tail (C_T) and the side group (C_S) are very similar in behavior for both carbons in the first coordination shell within r < 5.5 Å, indicating that both groups have similar hydration structure and exposure to water. Within a sphere of 5.5 Å, these groups have on average 14 water molecules. The snapshots in Figure 4c, as well as F-O_w correlations shown in Figure 5d, indicate that a significant number of F atoms of GenX molecules are interacting with water molecules. On average, within a 4.2 Å sphere each F atom interacts with about 5 water molecules despite the fact that the majority of GenX molecules are in micelles.

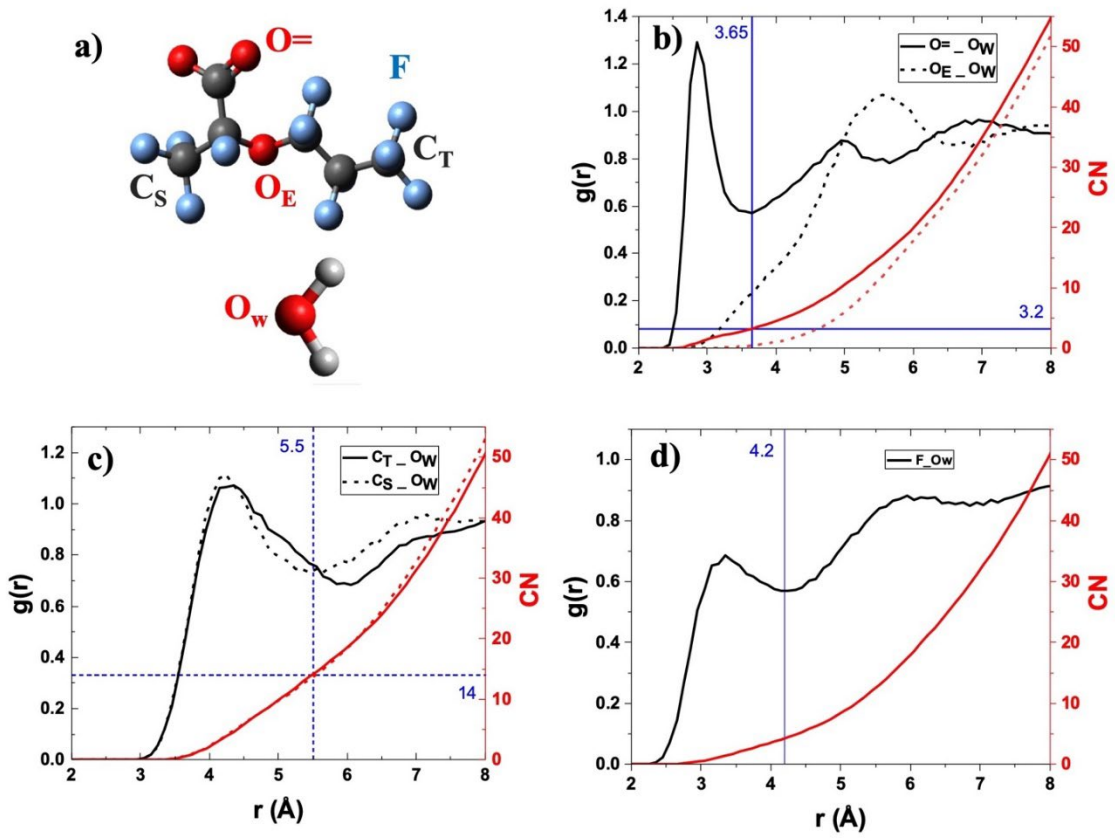

Figure 5. (a) Definition of atom types considered for radial distribution functions g(r) and coordination number CN, (b) comparison of O=-O_W and O_E-O_W g(r) and CN, (c) comparison of C_T-O_W and C_S-O_w g(r) and CN, and (d) F-O_W g(r) and CN obtained from MD simulations. Vertical lines indicate the distance defining the first coordination shell for each pair correlation, while horizontal lines show a corresponding CN in the first coordination shell.

It is interesting to examine the extent of hydration of GenX molecules. This information is important for the environmental applications of GenX, and also useful in the fitting of SANS data. Using MD simulation trajectories, we have calculated how many water molecules are in contact with each GenX micelle. To consider a water molecule to be in contact with a micelle, the O_w should be within R_c distance from any GenX atom in the micelle. We have considered three values of R_c = 3.0, 3.5 and 4.0 Å, which fall between the values defining the boundaries of O and F atoms first coordination shells. Figure 6a shows the dependence of the number of water molecules hydrating the GenX micelle as a function of micelle association number, normalized by the number of GenX molecules in the micelle (i.e., per one GenX molecule). Figure 6b shows distributions of

these hydration numbers for each R_c and averaged for all micelle sizes. Note that in these calculations, if a water molecule was in contact with two different GenX molecules or atoms, then it was counted only once. As expected, for smaller size micelles, the number of hydrating waters per GenX molecule is higher but, as the size of the micelle increases, the average hydration number also increases. For the tighter definition of hydrating water (R_c = 3.0 Å) the number of hydrating water molecules saturates around 4 whereas, for the looser definition of interfacial water (R_c = 4.0 Å), it is around 12 waters per GenX molecule. These values of hydration can be considered as the lower and upper bounds for the average water hydration number.

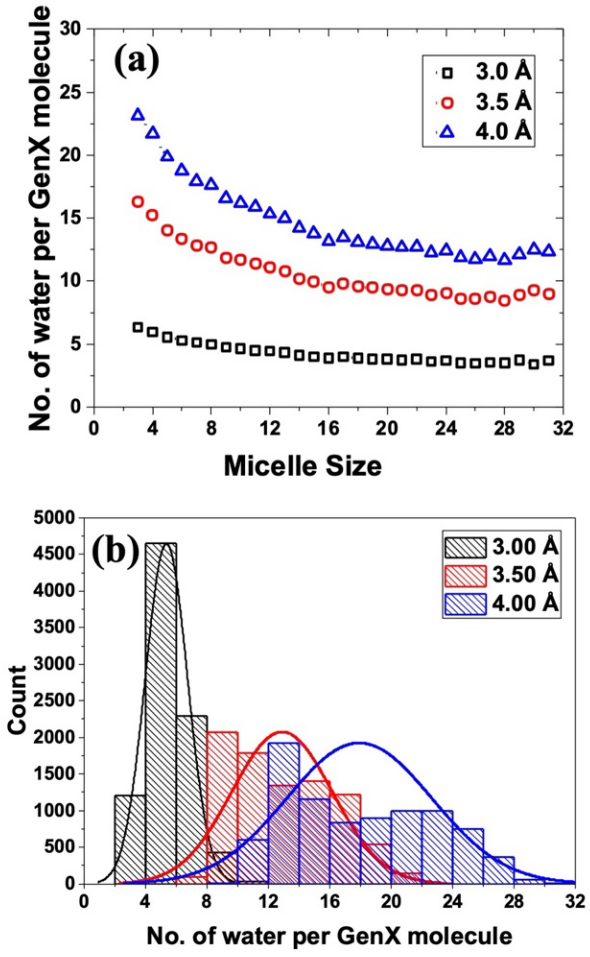

Figure 6. (a) Average number of water molecules in the first coordination shell of the micelle (defined using three cutoff radii: R_c = 3.0, 3.5 and 4.0 Å from any GenX atom) plotted as function of the micelle association number. (b) Distribution of hydrating waters per GenX molecule for three different cut off radii.

Another interesting structural feature to examine is how GenX molecules are oriented in the micelle. We have investigated the molecular orientation of each GenX molecule in micelles of different sizes by computing the angle (θ) between two vectors $\overrightarrow{v_1}$ and $\overrightarrow{v_2}$, where $\overrightarrow{v_1}$ is a vector between the center-of-mass of the micelle and the C_T group of the GenX molecule belonging to the micelle, while $\overrightarrow{v_2}$ is a vector from C_T to the carbon of the headgroup (Figure 7a). θ = 0˚ indicates that the GenX molecule tail is oriented toward the micelle center and the headgroup is radially outwards. θ = 90˚ corresponds to GenX molecules oriented tangentially to the surface of the micelle, while the 180˚ angle denotes that the GenX headgroup points inside the micelle core. The probability distribution of finding GenX molecule with θ orientation (normalized by sin(θ) to reflect the different phase space available for realization of each angle value) is shown in Fig. 7b. A broad peak around 90˚ indicates that GenX molecules prefer to align along the micelle surface.

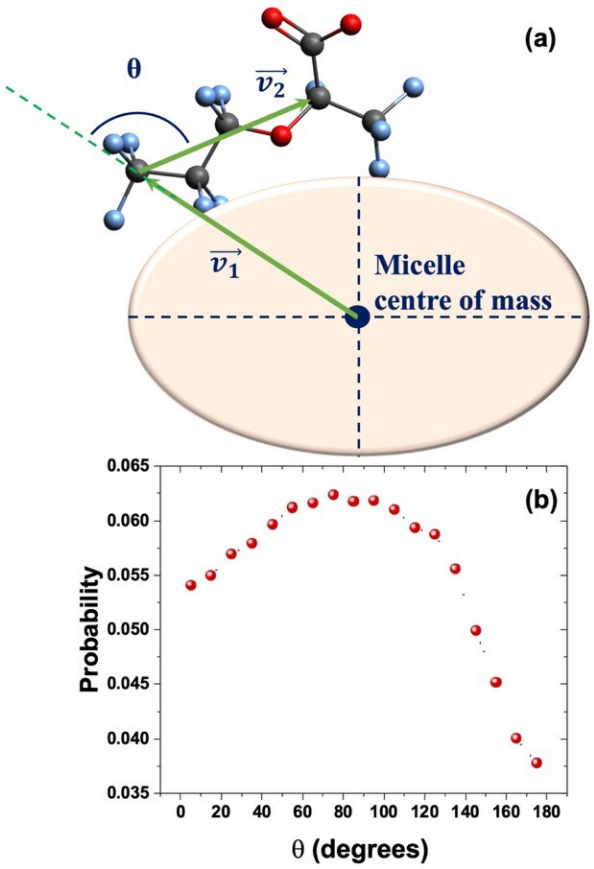

Figure 7. (a) Schematic representation of the method employed to compute the relative molecular orientation. The angle θ is between vector $\overrightarrow{v_1}$, which is from the center-of-mass of micelle to C_T, and the vector $\overrightarrow{v_2}$, which is from C_T to the carbon at the junction of headgroup and side-group. (b) Normalized distribution of computed molecular orientation (θ).

Viscosity. The hydration of GenX micelles can be experimentally assessed from viscosity measurements. Figure 8 shows the relative viscosity of aqueous solutions of GenX ammonium salt, plotted as a function of the micellized surfactant concentration (C-CMC) which accounts for the contribution to viscosity of only the micelles. A linear equation (Equation (4) neglecting the $k_1(v\phi)^2$ and $O(\phi)^3$ terms) was fitted to the viscosity measurement data set in Figure 8 and, from the x-coefficient value obtained, the hydrated volume of a GenX molecule V_s^{hyd} is calculated to 569.7 Å^3. After subtracting from this value the "dry" molecular volume of GenX (332.1 Å^3), the volume of the water hydrating a GenX molecule is estimated to 237.6 Å^3 which corresponds to ~8 water molecules. This number falls right in the middle between the upper and lower bounds of hydration numbers obtained from MD simulations, as discussed above in the context of Figure 6. The hydration number of NaPFHx or ammonium perfluorooctanoate (PFOA) reported in the literature is ~11 water molecules, 40% higher than the GenX hydration number (Kancharla *et al.*, 2019; Kancharla *et al.*, 2021b).

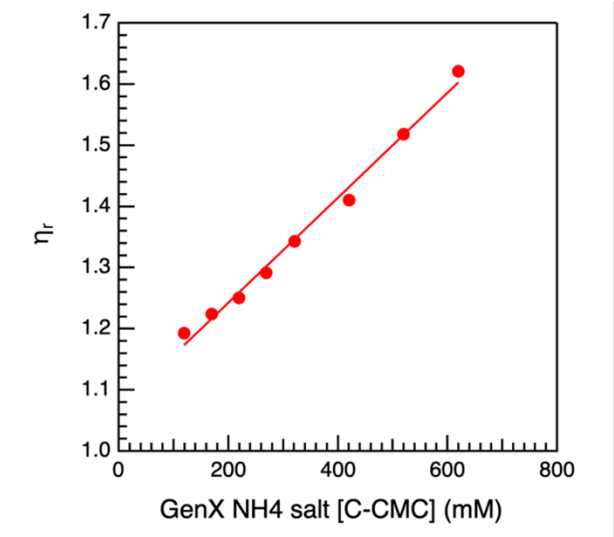

Figure 8. Relative viscosity of GenX ammonium salt aqueous solutions (21 °C) plotted as a function of micellized surfactant concentration. The line through the viscosity data points is fit to equation (4).

SANS analysis. When fitting SANS intensity data for GenX micelles in D_2O, we considered the micelle core to consist of $CF_3(CF_2)_2OCF$ chains and 0, 1, or 2 water molecules hydrating a $CF_3(CF_2)_2OCF$ chain (to account for GenX hydrophobic chain contact with water), and the shell to consist of carboxylate headgroups, CF_3 branch, counterions, and associated water molecules.

We assigned the CF_3 branch in the micelle shell following information from MD. Further, we fixed the total number of water molecules hydrating a GenX molecule in the micelle ($N_H + N_{H,O}$). Two cases have been considered, (i) $N_H + N_{H,O} = 8$, based on the GenX hydration number obtained from viscosity, and (ii) $N_H + N_{H,O} = 12$, based on upper bound of the GenX hydration number obtained from MD results. For instance, case (i) if $N_{H,O} = 0$, $N_H = 8$; $N_{H,O} = 1$, $N_H = 7$; $N_{H,O} = 2$, $N_H = 6$, and case (ii) if $N_{H,O} = 0$, $N_H = 12$; $N_{H,O} = 1$, $N_H = 11$; $N_{H,O} = 2$, $N_H = 10$.

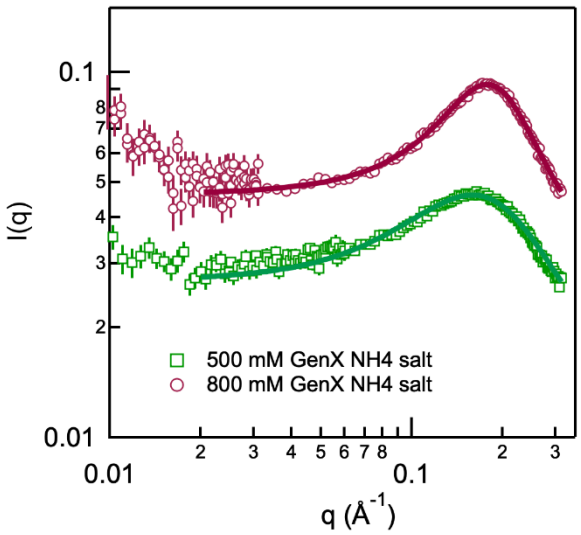

Figure 9. SANS intensity profiles of GenX ammonium salt in D_2O corrected for solvent (D_2O) scattering. Markers represent the experiment data and solid lines represent the fits using monodisperse core-shell ellipsoid model form factor with Hayter RMSA structure factor described in the text, considering 8 water molecules hydrating each GenX molecule in the micelle.

Figure 9 shows the SANS absolute intensity profiles of GenX ammonium salt in D_2O at 22 °C and the corresponding fits using the monodisperse core-shell ellipsoid form factor with Hayter rescaled MSA structure factor considering 8 water molecules hydrating each GenX molecule in the micelle. The correlation peak reflects repulsive interactions between the micelles. The intermicelle distance d can be estimated from the q value at the peak maximum $d = 2\pi/q_{max}$. Table 1 summarizes important parameters obtained by fitting GenX SANS data.

Table 1. Parameters obtained by fitting SANS intensity data of GenX ammonium salt in D_2O, corrected for solvent (D_2O) scattering, using the monodisperse core-shell ellipsoid form factor and the Hayter rescaled MSA structure factor, and considering the number of water molecules hydrating each GenX molecule in the micelle 8 (obtained from viscosity measurements). $N_{H,O}$ number of water molecules hydrating an oxygen atom in the core, N_{agg} association number (number of surfactant molecules per micelle); α fractional

charge or charge per surfactant molecule in a micelle; b micelle core minor radius; ε ratio of micelle core major to minor radius; δ shell thickness; R_{eq} equivalent spherical micelle radius; $V_{h,c}$ volume percentage of water in the micelle core; φ volume fraction of the micelles; d inter-micelle distance; and I_{peak} intensity at the correlation peak maximum. χ_R^2 is a statistical parameter that quantifies the differences between the calculated and experimental SANS data sets.

GenX (mM)	$N_{H,O}$	N_{agg}	α	b (Å)	ε	δ (Å)	R_{eq} (Å)	$V_{h,c}$ (%)	Φ	d (Å)	I_{peak}	χ_R^2
500	0	5.9 (±0.1)	0.72 (±0.03)	8.0	0.55 (±0.006)	2.7	9.35 (±0.02)	0	0.0519 (±0.002)	39.3	0.046	2.20
500	1	5.9 (±0.1)	0.75 (±0.03)	8.0	0.64 (±0.006)	2.4	9.34 (±0.02)	13	0.0519 (±0.001)	39.3	0.046	1.85
500	2	5.9 (±0.1)	0.78 (±0.03)	8.0	0.72 (±0.006)	2.1	9.33 (±0.02)	23	0.0522 (±0.001)	39.3	0.046	1.53
800	0	8.3 (±0.1)	0.93 (±0.03)	8.0	0.78 (±0.005)	3.1	10.45 (±0.02)	0	0.0883 (±0.001)	34.9	0.093	0.99
800	1	8.3 (±0.1)	0.96 (±0.03)	8.0	0.89 (±0.005)	2.7	10.44 (±0.02)	13	0.0909 (±0.001)	34.9	0.093	0.95
800	2	8.3 (±0.1)	0.99 (±0.03)	8.0	1.01 (±0.005)	2.4	10.45 (±0.02)	23	0.0939 (±0.001)	34.9	0.093	1.17

The average association number of GenX ammonium salt micelles in aqueous solution obtained from SANS is 5.9 at 500 mM GenX and 8.3 at 800 mM GenX, a 40% increase upon surfactant concentration increase from 500 to 800 mM. The GenX micelle size (R_{eq}) increased by 12%, the fractional charge on a micelle (α) (degree of counterion dissociation) increased by 28%, and the intermicelle distance decreased by 11% with the increase in GenX concentration from 500 to 800 mM. Our SANS results show that the ratio of the micelle core major to minor radius (ε) is smaller than 1, which means that the micelle core major radius is smaller than the extended length of surfactant (set to equal the micelle core minor radius). This is in good agreement with the tendency of GenX molecules to tilt along the micelle surface, established by MD (Figure 7). The average area per surfactant headgroup at the core-shell interface obtained from SANS parameters for the case of dry core ($N_{H,O}$ = 0) is 96.3 Å^2 for 500 mM GenX and 82.9 Å^2 for 800 mM GenX. These values are in excellent agreement with the A_{min} value obtained from the surface tension data.

SANS parameters obtained using the monodisperse core-shell ellipsoid form factor with Hayter rescaled MSA structure factor considering 12 water molecules (the upper bound hydration value

obtained from MD) hydrating each GenX molecule in the micelle are presented in SI (refer to Table S5) together with the corresponding fits. A comparison of GenX micelle parameters obtained considering 8 or 12 water molecules of hydration shows that the micelle association number, fractional charge, and axial ratio do not change, only the shell thickness (where water resides) increases by 20 – 30 %. Considering water in the micelle core ($V_{h,c}$ = 13% or 23%) resulted in no big difference in the micelle parameters.

We have also fitted SANS intensity data of GenX micelles using the monodisperse and polydisperse core-shell sphere form factor and Hayter rescaled MSA structure factor (results are presented in SI). The results obtained show that there is no difference in the GenX micelle association number, fractional charge, and size, whether we consider monodisperse core-shell sphere form factor or monodisperse core-shell ellipsoid form factor. Applying polydispersity to the radius of the micelle core, using the Schulz distribution, gave PD = 0.066 for 500 mM GenX and PD = 0.007 for 800 mM GenX, and there is no difference in the micelle parameters obtained when compared to monodisperse core-shell sphere fits. PD = σ/R_A is the ratio of the standard deviation of the core radius size distribution (σ) and the average micelle core radius (R_A) obtained from the fit. The low value of the polydispersity indicates that the system was essentially monodisperse. Small clusters contribute very little to the scattering intensity (refer to Figure S9).

Comparing the structure (obtained from SANS) of GenX micelles to that of NaPFHx micelles, both surfactants have 6 carbon atoms, however, NaPFHx forms larger micelles with N_{agg} = 14.7, ε = 1.41 and R_{eq} = 13 Å (Kancharla *et al.*, 2021b). This could be ascribed to the chemical structure of GenX. GenX has a CF_3 branch, whereas NaPFHx has a linear $CF_3(CF_2)_4$ chain. Comparing 6 carbon fluorinated surfactant micelles to 8 carbon fluorinated surfactant micelles, APFO forms ellipsoidal micelles with N_{agg} = 30, ε = 1.73, and R_{eq} = 17.6 Å (Dong *et al.*, 2021; Kancharla *et al.*, 2021a). APFO micelles have association number 5 times that of GenX micelles and 2 times that of NaPFHx micelles. The size of APFO micelles is 88% greater than that of GenX micelles, and 35% greater than NaPFHx micelles. For sodium perfluoroalkyl carboxylates, upon an increase in the hydrophobic part of the surfactant by 2 –CF_2– groups, the micelle association number increases by 70% and the size increases by 30% (Kancharla *et al.*, 2021b).

The SANS results of GenX forming small micelles with association number in the range 6 – 8 are in a very good agreement with the findings from MD. The ratio of micelle core major to minor radius (ε) < 1 indicates elongated micelles which agrees with the MD results. MD simulations have shown that, for association number = 7, radius of gyration (R_g) = 7.2 Å (Figure 6a), which is not far from the GenX micelle size (R_{eq}) obtained from SANS fits.

In the micelle composition that we considered while fitting the SANS data, the CF_3 side group of GenX is assigned to the micelle shell and is exposed to water, which is consistent with the MD results. MD simulations have shown that GenX molecules prefer to align along the micelle surface, and the CF_3 carbon atoms of the GenX tail are exposed to water. The SANS models that we used do not explicitly account for these. Having said this, the different models and micelle composition scenaria considered while fitting SANS data, including monodisperse sphere, monodisperse or polydisperse core-shell sphere with and without water in the micelle core, and monodisperse core-shell ellipsoid with and without water in the micelle core, all resulted in the same micelle parameters, lending confidence that these parameters describe well the GenX micelles.

We note that the surfactants properties reported here are for GenX in plain water. The presence in natural water of electrolytes or organic matter will modulate the surfactant association. For example, added NaCl decreased the CMC and increased the micelle size of PFOA, as we have recently shown (Kancharla et al., 2021b). We expect a similar trend in the case of GenX.

CONCLUSIONS

Emerging PFAS surfactants such as GenX have been introduced as less harmful alternatives to legacy PFAS (PFOA, PFOS) which are banned because they cause serious health issues. However, GenX is now present in waters and is generating concern as it has been found to adversely affect health. GenX is a surface-active molecule for which we know very little about its surfactant properties. The present study aims to fill this gap in knowledge.

Consistent and quantitative information on the formation and structure of GenX micelles emerges from analysis of experiments and MD simulations. Due to its short fluorocarbon chain, GenX has relatively high CMC (175 mM) and forms small micelles: association number of 6 – 8 and radius 10 Å. GenX molecules participating in micelles are hydrated by an average eight water molecules; the GenX anionic headgroup interacts strongly with water, whereas the ether oxygen is sterically hindered from water. The branched fluoroether chain of GenX is found 30% less hydrophobic than a linear fluorocarbon chain with the same number of carbon atoms. Having a linear $CF_3(CF_2)_4$ chain, NaPFHx forms larger micelles with association number = 15 and radius = 13 Å.

Self-assembly into micelles is a key feature of surfactants in aqueous solution. Analysis of CMC reveals specific contributions of hydrophobic tail and hydrophilic headgroup, while the micelle structure and composition provide information on how surfactants interact with themselves and with solvent (water) and other molecules present in solution. In a way, the micelles "amplify" subtle interactions that are always present, even if difficult to discern. Furthermore, the capability established in this study to predict from first principles micelle formation and structure confirms that such multiple and often competing interactions have been properly accounted for. This knowledge can be deployed to probe computationally other PFAS pollutants for which experimental results are lacking. A "simple" system as that examined here provides easier access to the fundamentals, and this helps the understanding of more complex systems encountered in environmental applications. Micelles are also relevant to environment and health in that PFAS surfactants, while typically found in very low bulk solution concentrations, they tend to concentrate a lot (partition) in the vicinity of surfaces in the context of separations (AC, ion exchange resins) and in the context of biointerfaces (proteins, lipid membranes).

This is the very first study of GenX micelles; further, this is the first MD study of surfactants with ether oxygen along the chain. The high-resolution structure and interactions knowledge presented here informs the GenX fate and transport in the aqueous environment, its interactions with various natural substances (e.g., minerals, humic acid) and biomolecules, and its binding to adsorbent materials. In a very recent study, photo-reductive destruction of GenX was significantly promoted when GenX was in the form of mixed micelles with hydroxyphenylacetic acids (hydrated electron precursors) and cetyl trimethyl ammonium bromide (Chen *et al.*, 2021).

Acknowledgements

This research was funded by the U.S. National Science Foundation (NSF), grant numbers CBET-1930959 and CBET-1930935. We acknowledge the support of the National Institute of Standards and Technology (NIST), U.S. Department of Commerce, in providing the neutron research facilities used in this work. Access to the CHRNS 30m Small-angle neutron scattering instrument was provided by the Center for High Resolution Neutron Scattering (CHRNS), a partnership between NIST and NSF under Agreement No. DMR-1508249. We thank Dr. Yimin Mao at NIST for valuable assistance with the SANS data acquisition. We thank Honeywell Buffalo Research Labs (Greg Smith and Roy Robinson) for providing access to a surface tension instrument.

REFERENCES

Allendorf, F., Berger, U., Goss, K.-U., Ulrich, N., 2019. Partition coefficients of four perfluoroalkyl acid alternatives between bovine serum albumin (BSA) and water in comparison to ten classical perfluoroalkyl acids. Environmental Science-Processes & Impacts. 21, 1852-1863.

Alves, A.V., Tsianou, M., Alexandridis, P., 2020. Fluorinated Surfactant Adsorption on Mineral Surfaces: Implications for PFAS Fate and Transport in the Environment. Surfaces. 3, 516-566.

Ateia, M., Arifuzzaman, M., Pellizzeri, S., Attia, M.F., Tharayil, N., Anker, J.N., Karanfil, T., 2019. Cationic polymer for selective removal of GenX and short-chain PFAS from surface waters and wastewaters at ng/L levels. Water Research. 163, 114874-114885.

Bao, Y., Deng, S., Jiang, X., Qu, Y., He, Y., Liu, L., Chai, Q., Mumtaz, M., Huang, J., Cagnetta, G., Yu, G., 2018. Degradation of PFOA Substitute - GenX (HFPO-DA ammonium salt) : Oxidation with UV/Persulfate or Reduction with UV/Sulfite? Environmental Science & Technology. 52, 11728.

Barzen-Hanson, K.A., Roberts, S.C., Choyke, S., Oetjen, K., McAlees, A., Riddell, N., McCrindle, R., Ferguson, P.L., Higgins, C.P., Field, J.A., 2017. Discovery of 40 Classes of Per- and Polyfluoroalkyl Substances in Historical Aqueous Film-Forming Foams (AFFFs) and AFFF-Impacted Groundwater. Environmental Science & Technology. 51, 2047-2057.

Bedrov, D., Piquemal, J.-P., Borodin, O., MacKerell, A.D., Roux, B., Schröder, C., 2019. Molecular Dynamics Simulations of Ionic Liquids and Electrolytes Using Polarizable Force Fields. Chemical Reviews. 119, 7940-7995.

Beekman, M., Zweers, P., Muller, A., DeVries, W., Janssen, P., Zeilmaker, M., 2016. Evaluation of substances used in the GenX technology by Chemours, Dordrecht. in, Rijksinstituut voor Volksgezondheid en Milieu (RIVM) Letter report, Vol. 0174, pp. 1-92.

Bentel, M.J., Yu, Y., Xu, L., Kwon, H., Li, Z., Wong, B.M., Men, Y., Liu, J., 2020. Degradation of Perfluoroalkyl Ether Carboxylic Acids with Hydrated Electrons: Structure–Reactivity Relationships and Environmental Implications. Environmental Science & Technology. 54, 2489-2499.

Berr, S.S., Jones, R.R.M., 1989. Small-angle neutron scattering from aqueous solutions of sodium perfluorooctanoate above the critical micelle concentration. Journal of Physical Chemistry. 93, 2555-2558.

Blake, B.E., Cope, H.A., Hall, S.M., Keys, R.D., Mahler, B.W., McCord, J., Scott, B., Stapleton, H.M., Strynar, M.J., Elmore, S.A., Fenton, S.E., 2020. Evaluation of Maternal, Embryo, and Placental Effects in CD-1 Mice following Gestational Exposure to Perfluorooctanoic Acid (PFOA) or Hexafluoropropylene Oxide Dimer Acid (HFPO-DA or GenX). Environmental Health Perspectives. 128, 27006.

Bodratti, A.M., Sarkar, B., Alexandridis, P., 2017. Adsorption of poly(ethylene oxide)-containing amphiphilic polymers on solid-liquid interfaces: Fundamentals and applications. Advances in Colloid and Interface Science. 244, 132-163.

Borodin, O., 2009. Polarizable Force Field Development and Molecular Dynamics Simulations of Ionic Liquids. Journal of Physical Chemistry B. 113, 11463-11478.

Brandsma, S.H., Koekkoek, J.C., van Velzen, M.J.M., de Boer, J., 2018. The PFOA substitute GenX detected in the environment near a fluoropolymer manufacturing plant in the Netherlands. Chemosphere. 220, 493.

Brase, R.A., Mullin, E.J., Spink, D.C., 2021. Legacy and emerging per- and polyfluoroalkyl substances: analytical techniques, environmental fate, and health effects. International Journal of Molecular Sciences. 22, 995.

Brusseau, M.L., 2019. The influence of molecular structure on the adsorption of PFAS to fluid-fluid interfaces: Using QSPR to predict interfacial adsorption coefficients. Water Research. 152, 148-158.

Buck, R.C., Franklin, J., Berger, U., Conder, J.M., Cousins, I.T., de Voogt, P., Jensen, A.A., Kannan, K., Mabury, S.A., van Leeuwen, S.P.J., 2011. Perfluoroalkyl and polyfluoroalkyl substances in the environment: Terminology, classification, and origins. Integrated Environmental Assessment and Management. 7, 513-541.

Buck, R.C., Murphy, P.M., Pabon, M., 2012. Chemistry, Properties, and Uses of Commercial Fluorinated Surfactants, in: T.P. Knepper, F.T. Lange (Eds.) Polyfluorinated Chemicals and Transformation Products. Springer Berlin Heidelberg, Berlin, Heidelberg, pp. 1-24.

Burkitt, S.J., Ottewill, R.H., Hayter, J.B., Ingram, B.T., 1987. Small angle neutron scattering studies on micellar systems part 1. Ammonium octanoate, ammonium decanoate and ammonium perfluoroocatanoate. Colloid & Polymer Science. 265, 619-627.

Caverly Rae, J.M., Craig, L., Slone, T.W., Frame, S.R., Buxton, L.W., Kennedy, G.L., 2015. Evaluation of chronic toxicity and carcinogenicity of ammonium 2,3,3,3-tetrafluoro-2-(heptafluoropropoxy)-propanoate in Sprague–Dawley rats. Toxicology Reports. 2, 939-949.

Chappell, G.A., Thompson, C.M., Wolf, J.C., Cullen, J.M., Klaunig, J.E., Haws, L.C., 2020. Assessment of the Mode of Action Underlying the Effects of GenX in Mouse Liver and Implications for Assessing Human Health Risks. Toxicologic Pathology. 48, 494-508.

Chen, Z., Teng, Y., Huang, L., Mi, N., Li, C., Ling, J., Gu, C., Jin, X., 2021. Rapid photo-reductive destruction of hexafluoropropylene oxide trimer acid (HFPO-TA) by a stable self-assembled micelle system of producing hydrated electrons. Chemical Engineering Journal. 420, 130436.

Cheng, W., Ng, C.A., 2018. Predicting Relative Protein Affinity of Novel Per- and Polyfluoroalkyl Substances (PFASs) by An Efficient Molecular Dynamics Approach. Environmental Science & Technology. 52, 7972-7980.

Conley, J.M., Lambright, C.S., Evans, N., McCord, J., Strynar, M.J., Hill, D., Medlock-Kakaley, E., Wilson, V.S., Gray, L.E., 2021. Hexafluoropropylene oxide-dimer acid (HFPO-DA or GenX) alters maternal and fetal glucose and lipid metabolism and produces neonatal mortality, low birthweight, and hepatomegaly in the Sprague-Dawley rat. Environment International. 146, 106204.

Coperchini, F., Croce, L., Denegri, M., Pignatti, P., Agozzino, M., Netti, G.S., Imbriani, M., Rotondi, M., Chiovato, L., 2020. Adverse effects of in vitro GenX exposure on rat thyroid cell viability, DNA integrity and thyroid-related genes expression. Environmental Pollution. 264, 114778.

Danish-EPA, 2015. Short-chain Polyfluoroalkyl Substances (PFAS). https://cswab.org/wp-content/uploads/2018/05/Short-chain-PFAS-literature-review-Danish-EPA-2015.pdf [accessed October 2021].

Dauchy, X., Boiteux, V., Bach, C., Rosin, C., Munoz, J.-F., 2017. Per- and polyfluoroalkyl substances in firefighting foam concentrates and water samples collected near sites impacted by the use of these foams. Chemosphere. 183, 53-61.

Dixit, F., Barbeau, B., Mostafavi, S.G., Mohseni, M., 2020. Efficient removal of GenX (HFPO-DA) and other perfluorinated ether acids from drinking and recycled waters using anion exchange resins. Journal of Hazardous Materials. 384, 121261.

Domingo, J.L., Nadal, M., 2019. Human exposure to per- and polyfluoroalkyl substances (PFAS) through drinking water: A review of the recent scientific literature. Environ Res. 177, 108648.

Dong, D., Kancharla, S., Hooper, J., Tsianou, M., Bedrov, D., Alexandridis, P., 2021. Controlling the self-assembly of perfluorinated surfactants in aqueous environments. Physical Chemistry Chemical Physics. 23, 10029-10039.

DuPont, 2010. DuPont™ GenX Processing Aid for Making Fluoropolymer Resins. https://bladenonline.com/wp-content/uploads/2017/06/Chemours_GenX_Brochure_Final_07July2010.pdf [accessed October 2021].

EPA, 2016. Drinking Water Health Advisories for PFOA and PFOS. https://www.epa.gov/ground-water-and-drinking-water/drinking-water-health-advisories-pfoa-and-pfos.

EPA, 2021. Human Health Toxicity Assessments for GenX Chemicals. https://www.epa.gov/chemical-research/human-health-toxicity-assessments-genx-chemicals [accessed October 2021].

Fajalia, A.I., Tsianou, M., 2014. Charging and uncharging a neutral polymer in solution: A small-angle neutron scattering investigation. Journal of Physical Chemistry B. 118, 10725-10739.

Fenton, S.E., Ducatman, A., Boobis, A., DeWitt, J.C., Lau, C., Ng, C., Smith, J.S., Roberts, S.M., 2021. Per- and Polyfluoroalkyl Substance Toxicity and Human Health Review: Current State of Knowledge and Strategies for Informing Future Research. Environmental Toxicology and Chemistry. 40, 606-630.

Gannon, S.A., Fasano, W.J., Mawn, M.P., Nabb, D.L., Buck, R.C., Buxton, L.W., Jepson, G.W., Frame, S.R., 2016. Absorption, distribution, metabolism, excretion, and kinetics of 2,3,3,3-tetrafluoro-2-(heptafluoropropoxy)propanoic acid ammonium salt following a single dose in rat, mouse, and cynomolgus monkey. Toxicology. 340, 1-9.

Gebbink, W.A., van Asseldonk, L., van Leeuwen, S.P.J., 2017. Presence of emerging per- and polyfluoroalkyl substances (PFASs) in river and drinking water near a fluorochemical production plant in the Netherlands. Environmental Science and Technology. 51, 11057–11065.

Glüge, J., Scheringer, M., Cousins, I.T., DeWitt, J.C., Goldenman, G., Herzke, D., Lohmann, R., Ng, C.A., Trier, X., Wang, Z., 2020. An overview of the uses of per- and polyfluoroalkyl substances (PFAS). Environmental Science: Processes & Impacts. 22, 2345-2373.

Gomis, M.I., Vestergren, R., Borg, D., Cousins, I.T., 2018. Comparing the toxic potency in vivo of long-chain perfluoroalkyl acids and fluorinated alternatives. Environment International. 113, 1-9.

Gomis, M.I., Wang, Z., Scheringer, M., Cousins, I.T., 2015. A modeling assessment of the physicochemical properties and environmental fate of emerging and novel per- and polyfluoroalkyl substances. Science of the Total Environment. 505, 981-991.

Guelfo, J.L., Adamson, D.T., 2018. Evaluation of a national data set for insights into sources, composition, and concentrations of per- and polyfluoroalkyl substances (PFASs) in U.S. drinking water. Environmental Pollution. 236, 505-513.

Heydebreck, F., Tang, J., Xie, Z., Ebinghaus, R., 2015. Alternative and Legacy Perfluoroalkyl Substances: Differences between European and Chinese River/Estuary Systems. Environmental Science & Technology. 49, 8386-8395.

Hoke, R.A., Ferrell, B.D., Sloman, T.L., Buck, R.C., Buxton, L.W., 2016. Aquatic hazard, bioaccumulation and screening risk assessment for ammonium 2,3,3,3-tetrafluoro-2-(heptafluoropropoxy)-propanoate. Chemosphere. 149, 336-342.

Hoover, W.G., 1985. Canonical dynamics: Equilibrium phase-space distributions. Physical Review A. 31, 1695-1697.

Hopkins, Z.R., Sun, M., DeWitt, J.C., Knappe, D.R.U., 2018. Recently detected drinking water contaminants: GenX and other per- and polyfluoroalkyl ether acids. Journal - American Water Works Association. 110, 13-28.

Huang, P.-J., Hwangbo, M., Chen, Z., Liu, Y., Kameoka, J., Chu, K.-H., 2018. Reusable Functionalized Hydrogel Sorbents for Removing Long- and Short-Chain Perfluoroalkyl Acids (PFAAs) and GenX from Aqueous Solution. ACS Omega. 3, 17447-17455.

Iijima, H., Kato, T., Yoshida, H., Imai, M., 1998. Small-angle X-ray and neutron scattering from dilute solutions of cesium perfluorooctanoate. Micellar growth along two dimensions. Journal of Physical Chemistry B. 102, 990-995.

Ito, A., Sakai, H., Kondo, Y., Yoshino, N., Abe, M., 1996. Micellar Solution Properties of Fluorocarbon−Hydrocarbon Hybrid Surfactants. Langmuir. 12, 5768-5772.

ITRC, 2020. Interstate Technology & Regulatory Council (ITRC). 2020. PFAS Technical and Regulatory Guidance Document and Fact Sheets. https://pfas-1.itrcweb.org/8-basis-of-regulations/ [accessed October 2021].

Ji, W., Xiao, L., Ling, Y., Ching, C., Matsumoto, M., Bisbey, R.P., Helbling, D.E., Dichtel, W.R., 2018. Removal of GenX and Perfluorinated Alkyl Substances from Water by Amine-Functionalized Covalent Organic Frameworks. Journal of American Chemical Society. 140, 12677-12681.

Jin, C., Yan, P., Wang, C., Xiao, J.-X., 2005. Effect of counterions on fluorinated surfactants 1. Surface activity and micellization. Acta Chimica Sinica. 63, 279-282.

Kalyanasundaram, K., 1988. Pyrene fluorescence as a probe of fluorocarbon micelles and their mixed micelles with hydrocarbon surfactants. Langmuir. 4, 942-945.

Kancharla, S., Bedrov, D., Tsianou, M., Alexandridis, P., 2022. Structure and composition of mixed micelles formed by nonionic block copolymers and ionic surfactants in water determined by small-angle neutron scattering with contrast variation. Journal of Colloid and Interface Science. DOI: 10.1016/j.jcis.2021.1010.1176.

Kancharla, S., Canales, E., Alexandridis, P., 2019. Perfluorooctanoate in Aqueous Urea Solutions: Micelle Formation, Structure, and Microenvironment. International Journal of Molecular Sciences. 20, 5761.

Kancharla, S., Dong, D., Bedrov, D., Tsianou, M., Alexandridis, P., 2021a. Structure and Interactions in Perfluorooctanoate Micellar Solutions Revealed by Small-Angle Neutron Scattering and Molecular Dynamics Simulations Studies: Effect of Urea. Langmuir. 37, 5339-5347.

Kancharla, S., Jahan, R., Bedrov, D., Tsianou, M., Alexandridis, P., 2021b. Role of chain length and electrolyte on the micellization of anionic fluorinated surfactants in water. Colloids and Surfaces A: Physicochemical and Engineering Aspects. 628, 127313.

Kato, K., Kalathil, A.A., Patel, A.M., Ye, X., Calafat, A.M., 2018. Per- and polyfluoroalkyl substances and fluorinated alternatives in urine and serum by on-line solid phase extraction–liquid chromatography–tandem mass spectrometry. Chemosphere. 209, 338-345.

Kissa, E., 2001. Fluorinated Surfactants and Repellents, 2nd Edition. Marcel Dekker, Incorporated, New York.

Krafft, M.P., Riess, J.G., 2015. Selected physicochemical aspects of poly- and perfluoroalkylated substances relevant to performance, environment and sustainability-part one. Chemosphere. 129, 4-19.

Kronberg, B., Holmberg, K., Lindman, B., 2014. Surface Chemistry of Surfactants and Polymers. John Wiley & Sons, Incorporated, Somerset.

Lee, Y.-C., Wang, P.-Y., Lo, S.-L., Huang, C.P., 2017. Recovery of perfluorooctane sulfonate (PFOS) and perfluorooctanoate (PFOA) from dilute water solution by foam flotation. Separation and Purification Technology. 173, 280-285.

Lin, Y., Smith, T.W., Alexandridis, P., 2002. Adsorption of a Polymeric Siloxane Surfactant on Carbon Black Particles Dispersed in Mixtures of Water with Polar Organic Solvents. Journal of Colloid and Interface Science. 255, 1-9.

Lukyanova, V.A., Papina, T.S., 2013. Standard enthalpies of formation of perfluoro(2-methyl-3-oxa)hexanoic and perfluoro(2,5-dimethyl-3,6-dioxa)nonanoic acids. Russian Journal of Physical Chemistry A. 87, 340-341.

Malmberg, C.G., 1958. Dielectric constant of deuterium oxide. Journal of Research of the National Bureau of Standards. 60, 609-612.

Martyna, G.J., Tuckerman, M.E., Tobias, D.J., Klein, M.L., 1996. Explicit reversible integrators for extended systems dynamics. Molecular Physics. 87, 1117-1157.

Meng, P., Deng, S., Lu, X., Du, Z., Wang, B., Huang, J., Wang, Y., Yu, G., Xing, B., 2014. Role of Air Bubbles Overlooked in the Adsorption of Perfluorooctanesulfonate on Hydrophobic Carbonaceous Adsorbents. Environmental Science & Technology. 48, 13785-13792.

Mohamed, A., Amith, M., Nishanth, T., Tanju, K., 2019. The overlooked short- and ultrashort-chain poly- and perfluorinated substances: A review. Chemosphere. 220, 866-882.

Mullin, L., Katz, D.R., Riddell, N., Plumb, R., Burgess, J.A., Yeung, L.W.Y., Jogsten, I.E., 2019. Analysis of hexafluoropropylene oxide-dimer acid (HFPO-DA) by liquid chromatography-mass spectrometry (LC-MS): Review of current approaches and environmental levels. TrAC Trends in Analytical Chemistry. 118, 828-839.

Munoz, G., Liu, J., Vo Duy, S., Sauvé, S., 2019. Analysis of F-53B, Gen-X, ADONA, and emerging fluoroalkylether substances in environmental and biomonitoring samples: A review. Trends in Environmental Analytical Chemistry. 23, e00066.

Muto, Y., Esumi, K., Meguro, K., Zana, R., 1987. Aggregation behavior of mixed fluorocarbon and hydrocarbon surfactants in aqueous solutions. Journal of Colloid and Interface Science. 120, 162-171.

Nagarajan, R., 1982. Are large micelles rigid or flexible? A reinterpretation of viscosity data for micellar solutions. Journal of Colloid and Interface Science. 90, 477-486.

Nagarajan, R., 2002. Molecular packing parameter and surfactant self-assembly: The neglected role of the surfactant tail. Langmuir. 18, 31-38.

Nivaggioli, T., Alexandridis, P., Hatton, T.A., Yekta, A., Winnik, M.A., 1995. Fluorescence Probe Studies of Pluronic Copolymer Solutions as a Function of Temperature. Langmuir. 11, 730-737.

Palmer, B.J., 1993. Direct Application of Shake to the Velocity Verlet Algorithm. Journal of Computational Physics. 104, 470-472.

Pan, Y., Zhang, H., Cui, Q., Sheng, N., Yeung, L.W.Y., Sun, Y., Guo, Y., Dai, J., 2018. Worldwide Distribution of Novel Perfluoroether Carboxylic and Sulfonic Acids in Surface Water. Environmental Science & Technology. 52, 7621-7629.

Prevedouros, K., Cousins, I.T., Buck, R.C., Korzeniowski, S.H., 2006. Sources, fate and transport of perfluorocarboxylates. Environmental Science and Technology. 40, 32-44.

Prosser, A.J., Franses, E.I., 2001. Adsorption and surface tension of ionic surfactants at the air–water interface: review and evaluation of equilibrium models. Colloids and Surfaces A: Physicochemical and Engineering Aspects. 178, 1-40.

Shea, D., 2018. Proposed Drinking Water Health Advisory Value for GenX: 2, 3, 3, 3-tetrafluoro-2-(heptafluoropropoxy)-propanoic acid. https://www.chemours.com/en/-/media/files/corporate/shea-toxicology-analysis-2018-04.pdf [accessed October 2021].

Sun, M., Arevalo, E., Strynar, M., Lindstrom, A., Richardson, M., Kearns, B., Pickett, A., Smith, C., Knappe, D.R.U., 2016. Legacy and Emerging Perfluoroalkyl Substances Are Important Drinking Water Contaminants in the Cape Fear River Watershed of North Carolina. Environmental Science & Technology Letters. 3, 415-419.

Sun, S., Guo, H., Wang, J., Dai, J., 2019. Hepatotoxicity of perfluorooctanoic acid and two emerging alternatives based on a 3D spheroid model. Environmental Pollution. 246, 955-962.

Sunderland, E.M., Hu, X.C., Dassuncao, C., Tokranov, A.K., Wagner, C.C., Allen, J.G., 2019. A review of the pathways of human exposure to poly- and perfluoroalkyl substances (PFASs) and

present understanding of health effects. Journal of Exposure Science & Environmental Epidemiology. 29, 131-147.

Thompson, C.M., Fitch, S.E., Ring, C., Rish, W., Cullen, J.M., Haws, L.C., 2019. Development of an oral reference dose for the perfluorinated compound GenX. Journal of Applied Toxicology. 39, 1267-1282.

Wang, J., Niven, R.K., 2021. Unification of surface tension isotherms of PFOA or GenX salts in electrolyte solutions by mean ionic activity. Chemosphere. 280, 130715.

Wang, R., Wang, W., Maimaiti, A., Shi, H., Wu, R., Li, Z., Qi, D., Yu, G., Deng, S., 2019a. Adsorption behavior and mechanism of emerging perfluoro-2-propoxypropanoic acid (GenX) on activated carbons and resins. Chemical Engineering Journal. 364, 132-138.

Wang, W., Mi, X., Zhou, Z., Zhou, S., Li, C., Hu, X., Qi, D., Deng, S., 2019b. Novel insights into the competitive adsorption behavior and mechanism of per- and polyfluoroalkyl substances on the anion-exchange resin. Journal of Colloid and Interface Science. 557, 655-663.

Wang, Z., Cousins, I.T., Scheringer, M., Hungerbühler, K., 2013. Fluorinated alternatives to long-chain perfluoroalkyl carboxylic acids (PFCAs), perfluoroalkane sulfonic acids (PFSAs) and their potential precursors. Environment International. 60, 242-248.

Weiss-Errico, M.J., O'Shea, K.E., 2019. Enhanced host–guest complexation of short chain perfluoroalkyl substances with positively charged β-cyclodextrin derivatives. Journal of Inclusion Phenomena and Macrocyclic Chemistry. 95, 111-117.

Wen, Y., Mirji, N., Irudayaraj, J., 2020. Epigenetic toxicity of PFOA and GenX in HepG2 cells and their role in lipid metabolism. Toxicology in Vitro. 65, 104797.

Xiao, F., 2017. Emerging poly- and perfluoroalkyl substances in the aquatic environment: A review of current literature. Water Research. 124, 482-495.

Xing, H., Yan, P., Xiao, J.-X., 2013. Unusual location of the pyrene probe solubilized in the micellar solutions of tetraalkylammonium perfluorooctanoates. Soft Matter. 9, 1164-1171.

Yan, N., Ji, Y., Zhang, B., Zheng, X., Brusseau, M.L., 2020. Transport of GenX in Saturated and Unsaturated Porous Media. Environmental Science & Technology. 54, 11876-11885.

Yang, L., Alexandridis, P., 2000. Polyoxyalkylene Block Copolymers in Formamide−Water Mixed Solvents: Micelle Formation and Structure Studied by Small-Angle Neutron Scattering. Langmuir. 16, 4819-4829.

Zhang, M., Yamada, K., Bourguet, S., Guelfo, J., Suuberg, E.M., 2020. Vapor Pressure of Nine Perfluoroalkyl Substances (PFASs) Determined Using the Knudsen Effusion Method. Journal of Chemical & Engineering Data. 65, 2332-2342.

Zoeller, N., Blankschtein, D., 1998. Experimental determination of micelle shape and size in aqueous solutions of dodecyl ethoxy sulfates. Langmuir. 14, 7155-7165.